Motion transitions of falling plates via quasi-steady aerodynamics

Ruifeng Hu[1,*] and Lifeng Wang[2,†]
[1] *School of Mechano-Electronic Engineering, Xidian University, Xian 710071, China*
[2] *School of Aeronautic Science and Engineering, Beihang University, Beijing 100191, China*

In this paper, we study the dynamics of freely falling plates based on the Kirchhoff equation and quasi-steady aerodynamic model. Motion transitions among fluttering, tumbling along cusp-like trajectory, irregular and tumbling along straight trajectory are obtained by solving the dynamical equations. Phase diagrams spanned between non-dimensional moment of inertia and aerodynamic coefficients or aspect ratio are built to identify regimes for these falling styles. We also investigate the stability of fixed points and bifurcation scenarios. It is found that the transitions are all heteroclinic bifurcations and influence of fixed point stability is local.

PACS numbers: 47.85.Gj, 05.45.Pq

1. INTRODUCTION

The problem of freely falling plate has attracted attention of scientific community since Maxwell [1]. This subject can share quite a lot in common with winged seeds dispersal [2–4], meteorology [5], particle sedimentation [6], insect flapping flight [7], autorotation phenomenon [8], windborne debris flight [9] and freely falling or rising motion of other objects in quiescent fluids [10–12].

There have been a lot of studies on this issue by experimental measurements [13–30] or numerical simulations based on computational fluid dynamics (CFD) [21, 31–36] or vortex method [37, 38]. Up to now, we already know that there are some different falling styles for a thin disk or plate determined by non-dimensional moment of inertia I^* and Reynolds number Re, i.e. steady falling, planar fluttering (zigzag), tumbling, spiral, and chaotic among others. Phase maps on which regimes for different falling styles are divided have been built in some studies [14, 17, 18, 25, 27, 35, 36].

It is difficult to investigate the dynamics and bifurcations in detail through experimental or computational methods mentioned above. Otherwise a dynamical model based on quasi-steady approximation can work. Tanabe and Kaneko [39] adopted the classical Kutta-Joukowski theorem to model lift, and assumed dissipative drag proportional tovelocity and dissipative torque proportional to angular velocity. Belmonte *et al.* [19] used the same model for lift but assumed dissipative drag quadratic in velocity and dissipative torque quadratic in angular velocity. Kirchhoff equation [40–42] is a set of differential equations which determines the motion of a solid body in an ideal fluid, and circulation as well as dissipative force and torque should be modeled in a real viscous flow. Mahadevan [43] employed a constant circulation model, while Wang and her colleagues [21, 44] suggested a circulation model consists of translational and rotational components which has been successfully applied in other studies [45–48]. Andersen *et al.* [49] made an analysis on the motion transitions based on their dynamical model and concluded that a heteroclinic bifurcation occurs at the transition between fluttering and tumbling. However, the wide transition region of irregular motion between fluttering and tumbling discovered in experiments and simulations was not observed in their study.

Although quasi-steady model provides us a powerful tool, it has limitations. As stated by Andersen *et al.* [21], the unsteady and historical wake effect is regarded to be poorly modeled by the existed quasi-steady approaches. A new approximate model considering this effect may improve the predicting capability of quasi-steady approach significantly, like what Ern *et al.* [50] have done for oblate axisymmetric bodies. However, it is beyond the scope of present paper and needs great effort to study in future.

There are some undetermined aerodynamic coefficients in the dynamical model of Andersen *et al.* [49] but their influences on the falling dynamics of plates was rarely considered. In the present study, we adopt the quasi-steady aerodynamic model of Andersen *et al.* [49] and include aspect ratio effect [29] to investigate the influences of aerodynamic coefficients and aspect ratio on the dynamics and bifurcation scenarios of freely falling plates. Plate is assumed with elliptical cross section, for which chord length is $2a$, maximum thickness $2b$, span length w and density ρ_s. The controlling dimensionless parameters includes aspect ratio $\lambda = w/2a$, thickness ratio $\beta = b/a$, density ratio $\epsilon = \rho_s/\rho_f$ (ρ_f is fluid density), non-dimensional moment of inertia $I^* \approx \epsilon\beta/2$ for very thin plate with elliptical cross section ($b \ll a$). Another key controlling dimensionless parameter is the Reynolds number, which can be defined based on the terminal velocity V_T ($V_T = \sqrt{(\rho_s/\rho_f - 1)gb}$) as $Re_T = V_T a/\nu$, or based on the average descending velocity $\bar{V}$ as $Re = \bar{V}a/\nu$, where ν is kinematic viscosity of a fluid.

The paper is arranged as follows. In Sec. 2, we describe the dynamical equations for falling plate with finite wingspan. Then we perform discussions and comments on aerodynamic coefficients is Sec. 3. Phase diagrams between non-dimensional moment of inertia I^* and aero-

*rfhu@xidian.edu.cn
†Author for correspondence: li_feng_wang@126.com

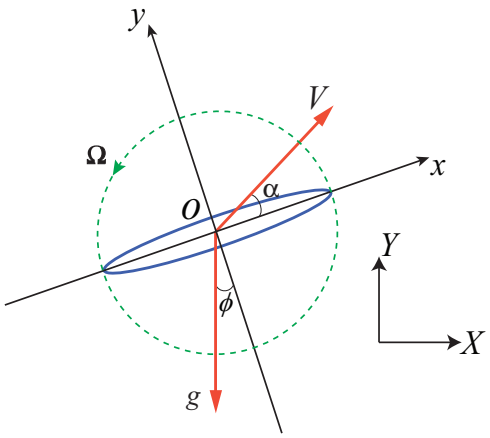

FIG. 1: (Color online) Schematic illustration of a plate with elliptical cross section and coordinate frames.

dynamic coefficients or aspect ratio λ are given in Sec. 4. The stability and bifurcation scenarios are analyzed in Sec. 5 and we summarize the main results in Sec. 6 finally.

2. DYNAMICAL MODEL

In Fig. 1, the laboratory coordinate frame OXY and co-rotating frame Oxy are sketched. The orientation angle ϕ is defined as the angle between the gravity and negative y axis, as well as the angle of attack α between velocity and positive x axis. The angular velocity of plate is $\Omega = \dot{\phi}$. Velocity components V_x and V_y in the OXY system can be transformed from those of u and v in Oxy system by $V_x = u\cos\phi - v\sin\phi$ and $V_y = u\sin\phi + v\cos\phi$. The total velocity is $V = \sqrt{u^2+v^2}$, and relations for velocity and angle of attack α are $\sin\alpha = v/V$ and $\cos\alpha = u/V$.

Based on the Kirchhoff equation [40, 41], the dynamical equations for freely falling plate are

$$(m+m_{11})\dot{u} = F_{a,x} - (L_T+L_R)\sin\alpha - (D_{i,T}+D_{i,R}+D_s)\cos\alpha - m'g\sin\phi, \quad (1)$$

$$(m+m_{22})\dot{v} = F_{a,y} + (L_T+L_R)\cos\alpha - (D_{i,T}+D_{i,R}+D_s)\sin\alpha - m'g\cos\phi, \quad (2)$$

$$(I+I_a)\dot{\Omega} = M_a - M_s, \quad (3)$$

$$\dot{\phi} = \Omega. \quad (4)$$

In Eqs. (1) and (2), $m = \pi\rho_s abw$ is the mass and $m' = \pi(\rho_s - \rho_f)abw$ the buoyancy-corrected mass of plate. $F_{a,x}$ and $F_{a,y}$ are components of added mass force in x and y directions, as $F_{a,x} = (m+m_{22})\Omega v$, $F_{a,y} = -(m+m_{11})\Omega u$ with $m_{11} = \pi\rho_f b^2 w$ and $m_{22} = \pi\rho_f a^2 w$ for plate with elliptical cross section. L_T and $D_{i,T}$ are lift and induced drag due to translational circulation, L_R and $D_{i,R}$ the lift and induced drag due to rotational circulation, and D_s the dissipative drag. In Eq. (3), $I = (\pi/4)\rho_s ab(a^2+b^2)w$ is the moment of inertia, and the added mass torque $M_a = (m_{11}-m_{22})uv$ as well as $I_a = (\pi/8)\rho_f(a^2-b^2)^2 w$ for plate with elliptical cross section. M_s is the dissipative torque. The expressions for the aerodynamic forces and torques are given in appendix A.

In order to obtain a dimensionless form of Eqs. (1) to (4), we define the length, velocity, and density scales as

$$L_{\rm ref} = a, \quad V_{\rm ref} = V_T, \quad \rho_{\rm ref} = \rho_f, \quad (5)$$

as well as the time scale $t_{\rm ref} = L_{\rm ref}/V_{\rm ref}$.

Then the dimensionless form of Eqs. (1) to (4) can be obtained as

$$\dot{u}^* = \frac{2I^*+1}{2I^*}\Omega v^* - \frac{1}{\pi I^*}\Big[-\frac{C_T V^{*2}\sin 2\alpha}{1+2C_T/\pi\lambda} + C_R\Omega V^*\Big]\cdot \sin\alpha - \frac{1}{\pi I^*}\Big[\frac{C_T^2 V^{*2}}{\pi\lambda(1+2C_T/\pi\lambda)^2} + C_R^2\Omega^2\frac{\ln(1+2\lambda)}{4\pi\lambda} + (A\sin^2\alpha + B\cos^2\alpha)V^{*2}\Big]\cos\alpha - \frac{\sin\phi}{2I^*}, \quad (6)$$

$$\dot{v}^* = -\frac{2I^*}{2I^*+1}\Omega u^* + \frac{2}{\pi(2I^*+1)}\Big[-\frac{C_T V^{*2}\sin 2\alpha}{1+2C_T/\pi\lambda} + C_R\Omega V^*\Big]\cos\alpha - \frac{2}{\pi(2I^*+1)}\Big[\frac{C_T^2 V^{*2}}{\pi\lambda(1+2C_T/\pi\lambda)^2} + C_R^2\Omega^2\frac{\ln(1+2\lambda)}{4\pi\lambda} + (A\sin^2\alpha + B\cos^2\alpha)V^{*2}\Big]\cdot \sin\alpha - \frac{\cos\phi}{2I^*+1}, \quad (7)$$

$$\dot{\Omega} = -\frac{2}{I^*+1/4}u^* v^* - \frac{2}{I^*+1/4}(\mu_1+\mu_2|\Omega|)\Omega, \quad (8)$$

$$\dot{\phi} = \Omega, \quad (9)$$

in which the β^2 term is omitted if $\beta \ll 1$. Variables with asterisk $(*)$ superscript indicate dimensionless parameters, such as $V^* = V/V_T$, $u^* = u/V_T$ and $v^* = v/V_T$. For the limiting case of $\lambda \to \infty$, the dimensionless equations Eqs. (6) to (9) are identical to those studied in [49] for two-dimensional problem.

3. AERODYNAMIC COEFFICIENTS

There are six undetermined aerodynamic coefficients, i.e. C_T, C_R, A, B, μ_1 and μ_2, in the quasi-steady aerodynamic model of Andersen *et al.* [21]. These coefficients

TABLE I: Values of the aerodynamic coefficients given in literature.

	C_T	C_R	A	B	μ_1	μ_2
Ref. [21]	1.0	1.0-1.4	2.0	0.08-0.28	0.0	0.16
Ref. [49]	1.2	π	2.4	0.4	0.2	0.2
Ref. [28]	4.5	1.8	0.5	0.2	0.0	0.15
Ref. [29]	π	1.8	–	–	0.7	0.7

are important and the Reynolds number enters into the problem through them implicitly.

In Table I, we display the values of these coefficients given in literature which were mostly obtained by fitting measurement data. Huang *et al.* [28] and Wang *et al.* [29] adopted close values for C_T and C_R other than Andersen *et al.* [21, 49]. The drag coefficients A and B used by Huang *et al.* [28] and Andersen *et al.* [21, 49] are in significant differences. Wang *et al.* [29] yielded much larger values of μ_1 and μ_2, which could be ascribed to the inclusion of the aerodynamic torque terms in their model.

In addition, Andersen *et al.* [21] compared measured aerodynamic forces and torques with quasi-steady model using measured kinematics other than solving the dynamical equations, and good coincidences were achieved. Huang *et al.* [28] demonstrated a direct comparison of trajectories between experimental measurement and solutions of dynamical equations, and qualitative agreements were observed but not quantitatively.

It is well known that the theoretical value of C_T equals to π for a thin airfoil at low angle of attack in steady incompressible flow [51]. Based on this, the translational circulation model of Andersen *et al.* [49] takes stall into account by $\Gamma_T = (1/2)C_T V c \sin 2\alpha$. In classical aerodynamics, we know that the lift coefficient of a wing section is not affected by Reynolds number very much in a wide range, so that C_T could be regarded to be nearly independent of Re.

According to the unsteady inviscid flow theory [52, 53], the lift of an airfoil undergoing small amplitude rotational oscillation is $\pi\rho_f V a^2\dot{\alpha} + 2\pi\rho_f V^2 a(1+\mathrm{i}k/2)C(k)\alpha$, where i is the square root of -1, k the reduced rotational frequency and $C(k)$ the Theodorsen's function. The term $\pi\rho_f V a^2\dot{\alpha}$ is the lift due to rotation and $2\pi\rho_f V^2(1+\mathrm{i}k/2)C(k)\alpha$ due to traditional translational circulation by non-zero angle of attack α. Then the theoretical value of C_R should be $\pi/2$ from that. We note that Munk [54] also deduced the lift for a pitching wing as $2\pi\rho_f V\Omega a^2$. The total lift obtained by Munk [54] includes two specific contributions which are equal in magnitude, i.e. one due to rotation and the other due to conventional translational circulation satisfying Kutta's condition. Thus C_R is given to be $\pi/2$ theoretically in another way. The Reynolds number effect on the lift of a rotating airfoil is not clear yet. While for the Magnus effect of a rotating circular cylinder, it is known that the aerodynamic force exhibits a significant dependency on Reynolds number when $\Omega a/V < 1.0$ and $Re \sim O(10^4)$, and the lift increases when Reynolds number decreases [55].

The dissipative force and torque coefficients A, B, μ_1 and μ_2 determine the magnitudes of dissipative effect on the motion of falling plate. A is the dissipative drag coefficient at $\alpha = \pi/2$. For a flat plate in normal flow, the drag coefficient varies with Reynolds number and reaches a peak at $Re = 300$ when $Re = 10^2 \sim 10^3$, and for $Re = 10^3 \sim 10^4$ the drag coefficient decreases when Re increases [56]. B is the drag coefficient at $\alpha = 0$ which is much smaller than A. As stated by Andersen *et al.* [49], the dissipative aerodynamic torque coefficients μ_1 and μ_2 may be more sensitive on the Reynolds number, and increase with decreasing Reynolds number. Whereas we do not know any quantitative relations between μ_1, μ_2 and Re.

In the following, we postulate $C_T = \pi$, $C_R = \pi/2$, $A = 2.4$, $B = 0.4$, $\mu_1 = \mu_2 = 0.2$ and $\lambda = 100$ if not stated.

4. PHASE DIAGRAMS

The trajectories of falling plates at different I^* by solving Eqs. (6) to (9) are shown in Fig. 2. By increasing I^*, the falling motions exhibit periodic fluttering, tumbling along cusp-like trajectory, irregular falling and tumbling along straight trajectory, respectively. In the experimental studies of Smith [17] and Belmonte *et al.* [19], a sharp transition boundary between fluttering and tumbling was identified without chaotic or irregular regime. It is noted that tip plates or rings were utilized to reduce the three-dimensional flow effects in their experiments, but we do not know if this is related to the disappearances of chaotic falling regime. Andersen *et al.* [21] performed measurement and successfully observed chaotic motion between fluttering and tumbling by increasing I^*. The tumbling motion along cusp-like trajectory at $I^* = 0.75$ as in Fig. 2 (b) is similar to that observed experimentally by Andersen *et al.* [21], for which pronounced gliding and fast rotation segments could be distinguished. The tumbling motion along straight trajectory at $I^* = 10$ in Fig. 2 (d) arises after a long steady falling stage, which was missed in the solutions of Andersen *et al.* [49].

Initial condition can affect the transient length after release. When plate is fluttering, irregular or tumbling in cusp-like trajectory, we found that the transient is longer for initial condition with edge-on descent than broadside-on one. While it is in a contrary manner when plate is tumbling in straight trajectory, initial condition with broadside-on descent produces longer transient. Moreover, the transient is shortened if an initial rotation of plate is imposed for all falling styles.

Next we compute the solutions of Eqs. (6) to (9) by varying the aerodynamic coefficients and aspect ratio, to reveal their effects on plate falling motion.

Fig. 3 shows phase diagram in the I^* versus C_R plane, with identification of fluttering, irregular and tumbling

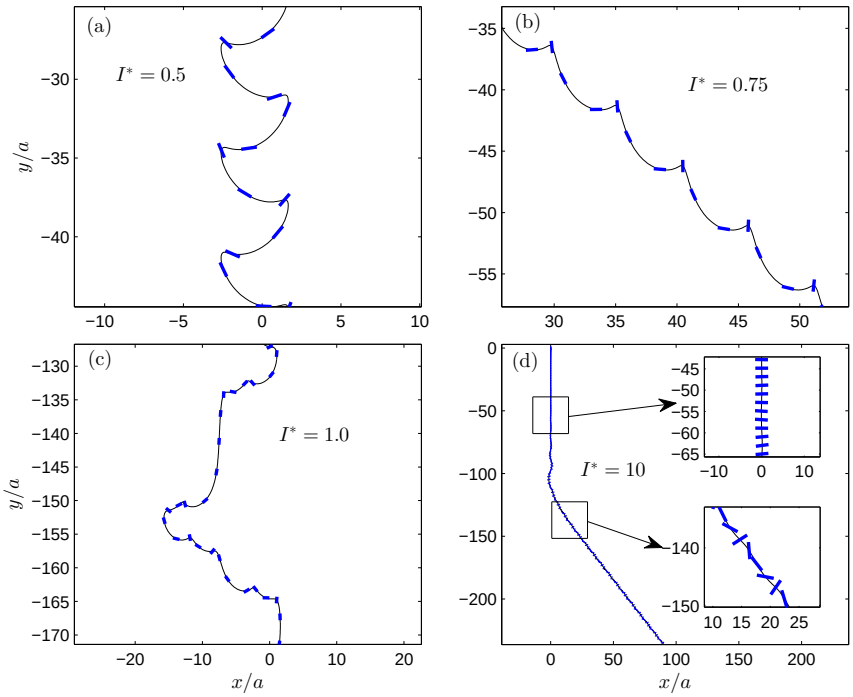

FIG. 2: (Color online) Solutions of plate trajectories with different I^*: (a) fluttering, (b) tumbling along cusp-like trajectory, (c) irregular and (d) tumbling along straight trajectory.

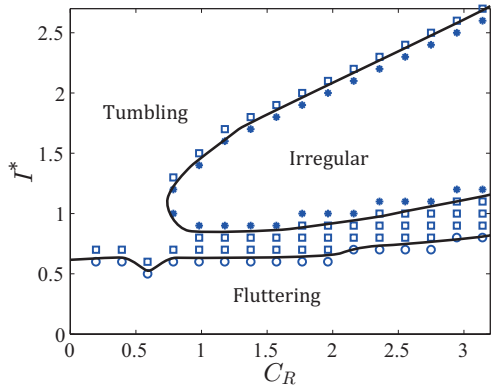

FIG. 3: (Color online) Phase diagram in the I^* versus C_R plane, showing fluttering (circles), irregular (stars) and tumbling (squares) regimes.

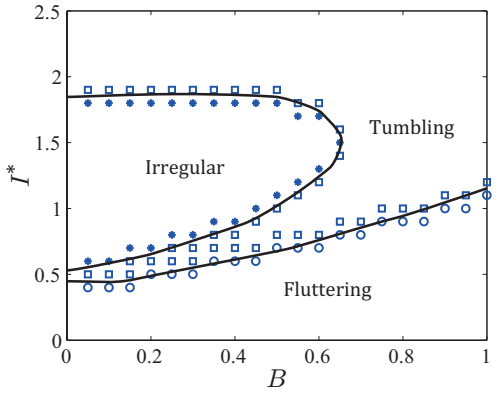

FIG. 4: (Color online) Phase diagram in the I^* versus B plane, showing fluttering (circles), irregular (stars) and tumbling (squares) regimes.

regimes. For small I^*, the plate motion is periodic fluttering as shown in Fig. 2(a). By increasing I^* the transition from fluttering to tumbling along cusp-like trajectory occurs, as displayed in Fig. 2(b). The falling motion could enter into the irregular regime by increasing I^* further, in which mixed fluttering and tumbling or even chaotic motion exists, if C_R is larger than $\pi/4$ or so, see Fig. 2(c). Finally, tumbling motion along straight trajectory can be achieved when I^* is larger. If I^* is large enough, the steady falling motion is observed firstly, then after a long distance it may be unstable and change into tumbling as displayed in Fig. 2(d).

We have computed the solutions with different A, and found its effect on the falling motion is not evident because the plate translates at low angle of attack in most of time. On the contrary, B plays a much significant role. Fig. 4 shows the phase diagram in the I^* versus B plane. The irregular falling regime arises if B is s-

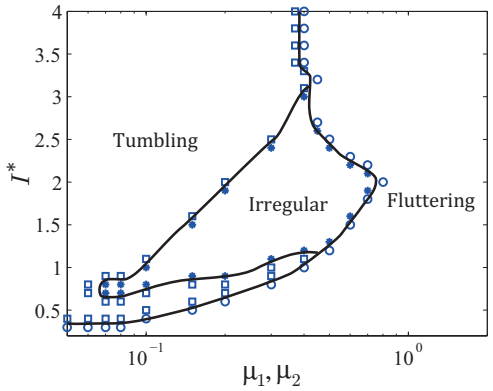

FIG. 5: (Color online) Phase diagram in the I^* versus μ plane, showing fluttering (circles), irregular (stars) and tumbling (squares) regimes.

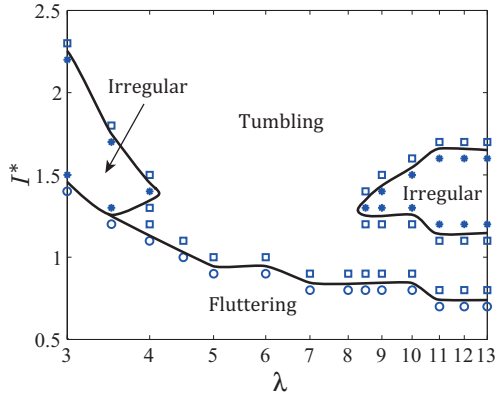

FIG. 6: (Color online) Phase diagram in the I^* versus λ plane, showing fluttering (circles), irregular (stars) and tumbling (squares) regimes.

maller than about 0.65. Fig. 5 shows the phase diagram in the I^* versus μ_1 ($\mu_1 = \mu_2$) plane. As μ_1 decreases, the plate falling motion may change from fluttering to tumbling, as well as irregular motion between them if $0.7 \leq \mu_1 = \mu_2 \leq 3.0$. Fig. 6 shows the phase diagram in the I^* versus λ plane. The irregular regime arises when aspect ratio λ in the ranges $\lambda \leq 4$ or $\lambda \geq 8.5$.

Wang *et al.* [29] studied the effect of aspect ratio λ on the motion of tumbling plate along straight trajectory. From Fig. 6 it is seen that aspect ratio λ may also influence falling styles of plates which has not been investigated yet. Therefore it is interesting to perform experimental observations or direct numerical simulations to find possible transitions of falling patterns by varying λ. We suggest that, according to the theoretical results in present study, people tests plates with small, moderate and large λ and increases I^* to see if they encounter different transition scenarios as in Fig. 6.

Falling patterns are determined by relative magnitudes of inertia and dissipative effects. Plate tumbling at turning points could be damped and changed into fluttering if the dissipative torque is large enough. Increasing C_R or B or decreasing λ can reduce the falling velocity then decrease the magnitude of the added mass term $-u^*v^*$ in Eq. (8), which indicates an increase of relative contribution of the dissipative torque. Therefore it can be outlined that, the plate falling style could be changed from fluttering to tumbling by decreasing C_R, μ_1, μ_2 or B, or increasing λ.

5. STABILITY AND BIFURCATION

As stated by Andersen *et al.* [49], there are four fixed points of Eqs. (6) to (9) with $\dot{u}^* = 0$, $\dot{v}^* = 0$, $\dot{\Omega} = 0$ and $\dot{\phi} = 0$ as

$$(u^*, v^*, \Omega, \phi)_{\text{fixed}} = \begin{cases} (0, -W, 0, 2n\pi), & \text{B1}, \\ (0, W, 0, (2n+1)\pi), & \text{B2}, \\ (-V, 0, 0, (2n+\frac{1}{2})\pi), & \text{E1}, \\ (V, 0, 0, (2n+\frac{3}{2})\pi), & \text{E2}, \end{cases}$$

in which n is an integer, B1 and B2 are broadside-on fixed points, E1 and E2 are end-on fixed points, and

$$W = \sqrt{\frac{\pi/2}{C_T^2/[\pi\lambda(1+2C_T/\pi\lambda)^2] + B}}, \tag{10}$$

$$V = \sqrt{\frac{\pi/2}{C_T^2/[\pi\lambda(1+2C_T/\pi\lambda)^2] + A}}. \tag{11}$$

The Jacobian matrix of right hands of dynamical equations Eqs. (6) to (9) is given in appendix B. We compute the eigenvalues of the matrix and show their real and imaginary parts versus the non-dimensional moment of inertia I^* for the edge-on fixed point E1 in Fig. 7 (the stability properties are the same for E1 and E2). The eigenvalues λ_1, λ_2, λ_3 and λ_4 are for u^*, v^*, Ω and ϕ directions respectively. λ_1 is always negative which implies a stable direction. λ_2 and λ_3 are a pair of conjugate complex when $I^* \leq 1.0$ and their real part are negative. For $1.0 \leq I^* \leq 1.2$, λ_2 and λ_3 are both negative real but not equal any more. λ_2 changes its stability to be positive at $I^* = 1.2$ while λ_3 keeps negative. After that, λ_2 returns to be stable while λ_3 loses its stability at $I^* = 1.52$. For λ_4, it is always real and becomes stable from unstable at $I^* = 1.2$. The stabilities of the broadside-on fixed points do not change for $0.2 \leq I^* \leq 2$.

In the following we analyze the bifurcation scenarios of transitions in Fig. 2, namely the transitions from fluttering to tumbling along cusp-like trajectory, from tumbling along cusp-like trajectory to irregular and from irregular to tumbling along straight trajectory, respectively.

The transition from fluttering to tumbling motion a-

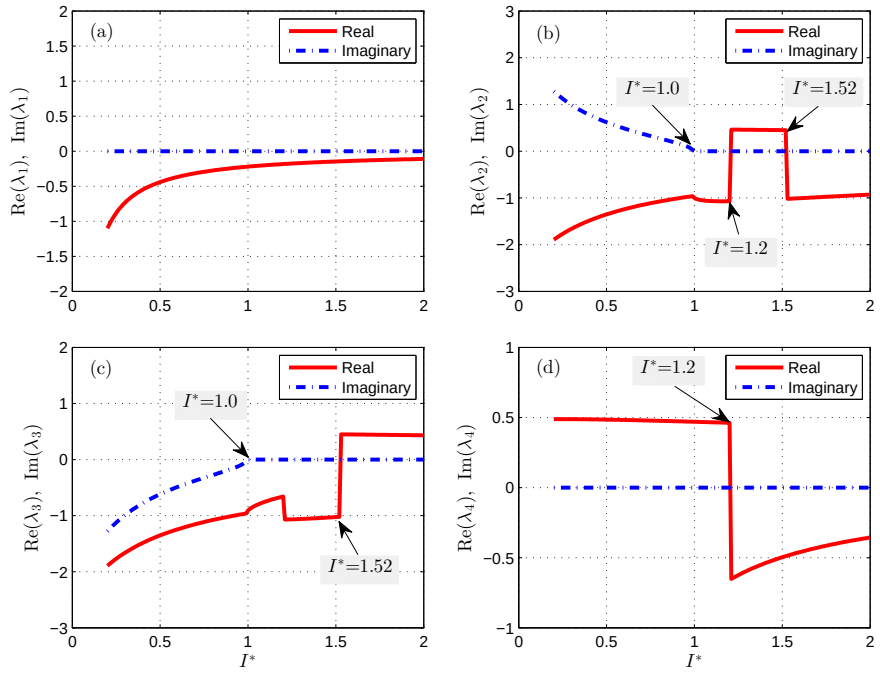

FIG. 7: (Color online) Eigenvalues of edge-on fixed point versus non-dimensional moment of inertia.

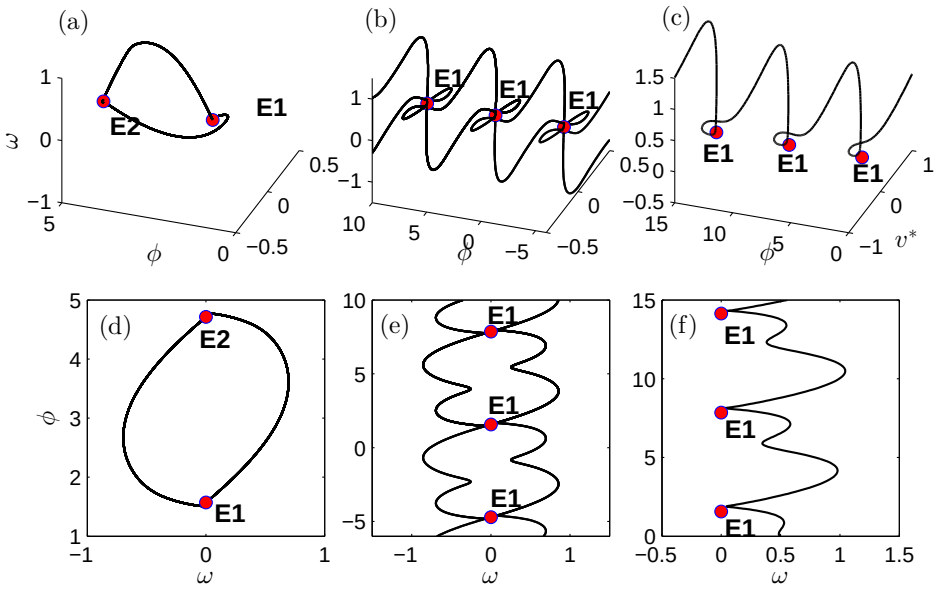

FIG. 8: (Color online) Phase trajectories for falling plate with (a,d) $I^*_{c1} = 0.6534$, (b,e) $I^*_{c2} = 0.8790$ and (c,f) $I^*_{c3} = 1.8390$.

long cusp-like trajectory occurs at $I^*_{c1} \approx 0.6534$, and the phase trajectory near edge-on fixed points is plotted in Fig. 8(a). A heteroclinic cycle connecting fixed points E1 and E2 is observed, which is indeed the same to that reported by Andersen *et al.* [49]. The eigenvalues of the Jacobian matrix at the fixed points are $\lambda_1 = -0.3370$, $\lambda_{2,3} = -1.1929 \pm 0.4259$i and $\lambda_4 = 0.4809$, indicating the Shil'nikov phenomenon [49, 57, 58].

The transition from tumbling along cusp-like trajectory to irregular motion arises at $I^*_{c2} \approx 0.8790$, and the phase trajectory near edge-on fixed points is shown in Fig. 8(b). At the bifurcation point $I^* = I^*_{c2}$, closed het-

eroclinic orbits connecting edge-on fixed points E1 are formed. The Shil'nikov phenomenon also exists because the eigenvalues are $\lambda_1 = -0.2505$, $\lambda_{2,3} = -1.0255 \pm 0.1962$i and $\lambda_4 = 0.4737$. If $I^*_{c1} < I^* < I^*_{c2}$, the phase trajectory of tumbling along cusp-like trajectory is similar to that of the tumbling along straight trajectory as shown in Fig. 8(c).

The transition from irregular motion happens at $I^*_{c3} \approx 1.8390$, and the phase trajectory near edge-on fixed points is shown in Fig. 8(c). It can be seen that there exist open heteroclinic orbits connecting edge-on fixed points E1. The Shil'nikov phenomenon is not observed any more and the eigenvalues of the Jacobian matrix are $\lambda_1 = -0.1197$, $\lambda_2 = -0.9591$, $\lambda_3 = 0.4381$ and $\lambda_4 = -0.3916$. The eigenvalue λ_3 is positive which means that the system is unstable in that direction.

The three transitions are all in occurrences of creation or destroy of heteroclinic cycles, so that they are all heteroclinic bifurcations. Stability changes of the edge-on fixed points in Fig. 7 indicate variations of local dynamics near fixed points other than affecting global behaviors and bifurcations. It should be further noted that there exists intermittency phenomenon near transition boundaries of the irregular motion, for which a short segment of irregular motion may arise intermittently in a long tumbling motion.

6. SUMMARY

We have studied the dynamics of freely falling plates with finite wingspan based on the Kirchhoff equation and quasi-steady aerodynamic model. By increasing non-dimensional moment of inertia I^*, we observed motion transitions from periodic fluttering, tumbling along cusp-like trajectory, irregular to tumbling along straight trajectory. Phase diagrams between I^* and aerodynamic coefficients or aspect ratio λ have been built, and various regimes for different falling styles are identified. We outline that the transitions are determined by relative magnitudes of inertia and dissipative effects, and the falling motion can be changed from fluttering to tumbling by decreasing C_R, μ_1, μ_2 or B, or increasing λ. We also studied the stability properties of fixed points with respect to I^* and the bifurcation scenarios at the transition boundaries. It has been found that the transitions mentioned above are all heteroclinic bifurcations, and the changes of fixed points stability are local which do not affect the global dynamics of plate falling motion.

Acknowledgments

This work is supported by the Fundamental Research Funds for the Central Universities of China (No. K5051304033). The authors are grateful for communications with Prof. Z. Jane Wang and discussions on dynamical systems with Dr K.M. Guo, as well as referee's helpful suggestions.

APPENDIX A: AERODYNAMIC FORCES AND TORQUES EXPRESSIONS

According to Wang *et al.* [29], the first order solution for the equation of the translational circulation considering trailing vortices effect is $A_1 = \alpha/(1 + 2\lambda/C_T)$. In this solution, the assumption $\sin 2\alpha_{eff} \approx 2\alpha_{eff}$ is taken for small effective angle of attack α_{eff} to obtain an analytical expression.

Here we assume a sinusoidal form for A_1 in place of the linear one with respect to the geometric angle of attack α and assure the asymptotic relation $C_{L,T} \to C_T \sin 2\alpha$ when $\lambda \to \infty$, so that

$$A_1 = \frac{\sin 2\alpha}{2 + \pi\lambda/C_T}. \tag{A1}$$

Eq. A1 is used to model the translational circulation as

$$\Gamma_T = -Va \cdot \pi\lambda A_1 = -\frac{C_T V a \sin 2\alpha}{1 + 2C_T/\pi\lambda}, \tag{A2}$$

and the translational lift and induced drag are

$$L_T = -\frac{\rho_f C_T V^2 a w \sin 2\alpha}{1 + 2C_T/\pi\lambda},\ D_{i,T} = \frac{\rho_f C_T^2 V^2 a w \sin^2 2\alpha}{\pi\lambda(1 + 2C_T/\pi\lambda)^2}. \tag{A3}$$

Also according to Wang *et al.* [29], the rotational lift and induced drag considering wing-tip vortex effect are

$$L_R = 2\rho_f C_R a^2 w \Omega V,\ D_{i,R} = \frac{2}{\pi}\rho_f C_R^2 a^4 \Omega^2 \ln(1 + 2\lambda). \tag{A4}$$

For the frictional dissipative drag coefficient, we follow Andersen *et al.* [21] to adopt a quadratic interpolation functions as

$$C_{Ds} = A \sin\alpha^2 + B \cos\alpha^2, \tag{A5}$$

where A and B are the drag coefficients at $\alpha = \pi/2$ and $\alpha = 0$ respectively.

The dissipative torque is given also following Andersen *et al.* [49] as

$$M_s = \pi\rho_f a^4 w \left(\frac{V_T}{a}\mu_1 + \mu_2|\Omega|\right)\Omega. \tag{A6}$$

APPENDIX B: THE JACOBIAN MATRIX

The Jacobian matrix of right hands of dynamical equations Eqs. (6) to (9) is

$$\mathbf{J} = \begin{bmatrix} J_{11} & J_{12} & J_{13} & J_{14} \\ J_{21} & J_{22} & J_{23} & J_{24} \\ J_{31} & J_{32} & J_{33} & 0 \\ 0 & 0 & 1 & 0 \end{bmatrix} \tag{B1}$$

with

$$J_{11}=\frac{\partial F_1}{\partial u^*}=\frac{2C_T}{\pi I^*(1+2C_T/\pi\lambda)}\frac{v^{*4}}{(u^{*2}+v^{*2})^{3/2}} - \frac{1}{\pi I^*}[\frac{C_T^2}{\pi\lambda(1+2C_T/\pi\lambda)^2}\frac{2u^{*2}+v^{*2}}{\sqrt{u^{*2}+v^{*2}}} + \frac{C_R^2\ln(1+2\lambda)}{4\pi\lambda}\frac{v^{*2}\Omega^2}{(u^{*2}+v^{*2})^{3/2}} + \frac{2Bu^{*4}+3Bu^{*2}v^{*2}+Av^{*4}}{(u^{*2}+v^{*2})^{3/2}}], \quad \text{(B2)}$$

$$J_{12}=\frac{\partial F_1}{\partial v^*}=(1+\frac{1}{2I^*})\Omega - \frac{1}{\pi I^*}[-\frac{2C_T}{1+2C_T/\pi\lambda}\frac{u^*v^*(2u^{*2}+v^{*2})}{(u^{*2}+v^{*2})^{3/2}}+C_R\Omega] - \frac{1}{\pi I^*}[\frac{C_T^2}{\pi\lambda(1+2C_T/\pi\lambda)^2}\frac{u^*v^*}{\sqrt{u^{*2}+v^{*2}}} - \frac{C_R^2\ln(1+2\lambda)}{4\pi\lambda}\frac{u^*v^*\Omega^2}{(u^{*2}+v^{*2})^{3/2}} + \frac{(2A-B)u^{*3}v^*+Au^*v^{*3}}{(u^{*2}+v^{*2})^{3/2}}], \quad \text{(B3)}$$

$$J_{13}=\frac{\partial F_1}{\partial\Omega}=(1+\frac{1}{2I^*}-\frac{C_R}{\pi I^*})v^* - \frac{C_R^2\ln(1+2\lambda)}{2\pi^2\lambda I^*}\frac{u^*\Omega}{\sqrt{u^{*2}+v^{*2}}}, \quad \text{(B4)}$$

$$J_{14}=\frac{\partial F_1}{\partial\phi}=-\frac{\cos\phi}{2I^*}, \quad \text{(B5)}$$

$$J_{21}=\frac{\partial F_2}{\partial u^*}=-\frac{2I^*}{2I^*+1}\Omega + \frac{2}{\pi(2I^*+1)}[-\frac{2C_T}{1+2C_T/\pi\lambda}\frac{u^*v^*(u^{*2}+2v^{*2})}{(u^{*2}+v^{*2})^{3/2}}+C_R\Omega] - \frac{2}{\pi(2I^*+1)}[\frac{C_T^2}{\pi\lambda(1+2C_T/\pi\lambda)^2}\frac{u^*v^*}{\sqrt{u^{*2}+v^{*2}}} - \frac{C_R^2\ln(1+2\lambda)}{4\pi\lambda}\frac{u^*v^*\Omega^2}{(u^{*2}+v^{*2})^{3/2}} + \frac{Bu^{*3}v^*+(2B-A)u^*v^{*3}}{(u^{*2}+v^{*2})^{3/2}}], \quad \text{(B6)}$$

$$J_{22}=\frac{\partial F_2}{\partial v^*}=-\frac{4C_T}{\pi(2I^*+1)(1+2C_T/\pi\lambda)}\frac{u^{*4}}{(u^{*2}+v^{*2})^{3/2}} - \frac{2}{\pi(2I^*+1)}[\frac{C_T^2}{\pi\lambda(1+2C_T/\pi\lambda)^2}\frac{u^{*2}+2v^{*2}}{\sqrt{u^{*2}+v^{*2}}} + \frac{C_R^2\ln(1+2\lambda)}{4\pi\lambda}\frac{u^{*2}\Omega^2}{(u^{*2}+v^{*2})^{3/2}} + \frac{Bu^{*4}+3Au^{*2}v^{*2}+2Av^{*4}}{(u^{*2}+v^{*2})^{3/2}}], \quad \text{(B7)}$$

$$J_{23}=\frac{\partial F_2}{\partial\Omega}=[-\frac{2I^*}{2I^*+1}+\frac{2C_R}{\pi(2I^*+1)}]u^* - \frac{C_R^2\ln(1+2\lambda)}{\pi^2\lambda(2I^*+1)}\frac{v^*\Omega}{\sqrt{u^{*2}+v^{*2}}}, \quad \text{(B8)}$$

$$J_{24}=\frac{\partial F_2}{\partial\phi}=\frac{\sin\phi}{2I^*+1}, \quad \text{(B9)}$$

$$J_{31}=\frac{\partial F_3}{\partial u^*}=-\frac{2v^*}{I^*+1/4}, \quad \text{(B10)}$$

$$J_{32}=\frac{\partial F_3}{\partial v^*}=-\frac{2u^*}{I^*+1/4}, \quad \text{(B11)}$$

$$J_{33}=\frac{\partial F_3}{\partial\Omega}=-\frac{2\left(\mu_1+2\mu_2|\Omega|\right)}{I^*+1/4}, \quad \text{(B12)}$$

in which F_1, F_2 and F_3 are the right hands of Eq. (6), Eq. (7) and Eq. (8) respectively.

[49] Andersen A, Pesavento U and Wang Z J 2005*a* *J. Fluid Mech.* **541**, 91–104.

[21] Andersen A, Pesavento U and Wang Z J 2005*b* *J. Fluid Mech.* **541**, 65–90.

[51] Anderson J D 2001 *Fundamentals of aerodynamics* 3rd edition edn McGraw-Hill.

[42] Aref H and Jones S W 1993 *Phys. Fluids A* **5**(12), 3026–3028.

[3] Augspurger C K 1986 *Am. J. Bot.* **73**, 353–363.

[35] Auguste F, Magnaudet J and Fabre D 2013 *J. Fluid*

Mech. **719**, 388–405.
[19] Belmonte A, Eisenberg H and Moses E 1998 *Phys. Rev. Lett.* **81**, 345–348.
[46] Bergou A J, Xu S and Wang Z J 2007 *J. Fluid Mech.* **591**, 321–337.
[45] Berman G J and Wang Z J 2007 *J. Fluid Mech.* **582**, 153–168.
[52] Biot M A 1942 *J. Aeronaut. Sci.* **9**, 186–190.
[33] Bönisch S and Heuveline V 2007 *Comput. Fluids* **36**, 1434–1445.
[15] Bustamante A C and Stone G W 1969 *in* 'Proceedings of the AIAA 7th Aerospace Sciences Meeting' New York, NY.
[36] Chrust M, Bouchet G and Dûsek J 2013 *Phys. Fluids* **25**, 044102.
[6] Davis R H and Acrivos A 1985 *Annu. Rev. Fluid Mech.* **17**, 91–118.
[13] Dupleich P 1941 Rotation in free fall of rectangular wings of elongated shape Technical Report 1201 NACA Tech. Mem.
[11] Ern P, Risso F, Fabre D and Magnaudet J 2012 *Annu. Rev. Fluid Mech.* **44**, 97–121.
[50] Ern P, Risso F, Fernandes P C and Magnaudet J 2009 *Phys. Rev. Lett.* **102**, 134505.
[22] Fernandes P C, Ern P, Risso F and Magnaudet J 2008 *J. Fluid Mech.* **606**, 209–223.
[18] Field S B, Klaus M, Moore M G and Nori F 1997 *Nature* **388**, 252–254.
[53] Fung Y C 1993 *An introduction to the theory of aeroelasticity* Dover.
[58] Guckenheimer J and Homes P 1983 *Nonlinear oscillations, dynamic systems, and bifurcations of vector fields* Springer.
[23] Hirata K, Shimizu K, Fukuhara K, Yamauchi K, Kawaguchi D and Funaki J 2009 *J. Fluid Sci. Tech.* **4**, 168–187.
[56] Hoerner S F 1965 *Fluid-dynamic drag: practical information on aerodynamic drag and hydrodynamic resistance* Hoerner Fluid Dynamics.
[28] Huang W T, Liu H, Wang F X, Wu J Q and Zhang H P 2013 *Phys. Rev. E* **88**, 053008.
[32] Jin C Q and Xu K 2008 *Commun. Comput. Phys.* **3**, 834–851.
[37] Jones M and Shelley M J 2005 *J. Fluid Mech.* **540**, 393–425.
[30] Kanso E, Heisinger L and Newton P 2014 *J. Fluid Mech.* **742**, 243–253.
[34] Kolomenskiy D and Schneider K 2010 *Theor. Comput. Fluid Dyn.* **24**, 169–173.
[40] Lamb H 1945 *Hydrodynamics* Dover.
[27] Lee C B, Su Z, Zhong H J, Chen S Y, Zhou M D and Wu J Z 2013 *J. Fluid Mech.* **732**, 77–104.
[4] Lentink D, Dickson W B, von Leeuwen J L and Dickinson M H 2009 *Science* **324**, 1438–1440.
[5] List R and Schemenauer R S 1971 *J. Atmos. Sci.* **28**, 110–115.
[8] Lugt H J 1983 *Annu. Rev. Fluid Mech.* **15**, 123–147.
[10] Magnaudet J and Eames I 2000 *Annu. Rev. Fluid Mech.* **32**, 659–708.
[43] Mahadevan L 1996 *C. R. Acad. Sci. Paris* **323**, 729–736.
[20] Mahadevan L, Ryu W S and Samuel A D T 1999 *Phys. Fluids* **11**, 1–3.
[1] Maxwell J C 1854 *Camb. Dublin Math. J.* **9**, 145–148.
[2] McCutchen C W 1977 *Science* **197**, 691–692.
[38] Michelin S and Smith S G L 2010 *Theor. Comput. Fluid Dyn.* **24**, 195–200.
[31] Mittal R, Seshadri V and Udaykumar H S 2004 *Theoret. Comput. Fluid Dyn.* **17**, 165–170.
[54] Munk M M 1925 Note on the air forces on a wing caused by pitching Technical Report 217 NACA Tech. Notes.
[48] Paoletti P and Mahadevan L 2011 *J. Fluid Mech.* **689**, 489–516.
[44] Pesavento U and Wang Z J 2004 *Phys. Rev. Lett.* **93**, 144501.
[41] Sedov L I 1965 *Two-dimensional Problems in Hydrodynamics and Aerodynamics* Interscience Publishers.
[57] Shil'nikov L P 1965 *Sov. Math. Dokl.* **6**, 163–166.
[17] Smith E H 1971 *J. Fluid Mech.* **50**, 513–534.
[16] Stringham G, Simons D B and Guy H P 1969 *The behavior of large particles falling in quiescent liquids* US Government Printing Office.
[55] Swanson W M 1961 *Journal of Basic Engineering* **83**(3), 461–470.
[9] Tachikawa M 1983 *J. Wind Eng. Ind. Aerodyn.* **14**(1), 443–453.
[24] Tam D, Bush J W M, Robitaille M and Kudrolli A 2010 *Phys. Rev. Lett.* **104**, 184504.
[39] Tanabe Y and Kaneko K 1994 *Phys. Rev. Lett.* **73**, 1372–1375.
[12] Varshney K, Chang S and Wang Z J 2013 *Phys. Rev. E* **87**, 053021.
[29] Wang W B, Hu R F, Xu S J and Wu Z N 2013 *J. Fluid Mech.* **733**, 650–679.
[7] Wang Z J 2005 *Annu. Rev. Fluid Mech.* **37**, 183–210.
[47] Whitney J P and Wood R J 2010 *J. Fluid Mech.* **660**, 197–220.
[14] Willmarth W W, Hawk N E and Harvey R L 1964 *Phys. Fluids* **7**, 197–208.
[25] Zhong H J, Chen S Y and Lee C B 2011 *Phys. Fluids* **23**, 011702.
[26] Zhong H J, Lee C B, Su Z, Chen S Y, Zhou M D and Wu J Z 2013 *J. Fluid Mech.* **716**, 228–250.